Struct Multidisc Optim 21, 196–208 

# Optimization of a hyper-elastic structure with multibody contact using continuum-based shape design sensitivity analysis

**N.H. Kim,Y.H. Park,, K.K. Choi**

**Abstract** In this paper, a continuum-based shape design sensitivity formulation is presented for a hyper-elastic structure with multibody frictional contact. A nearly incompressible constraint is treated using the pressure projection method that projects a hydrostatic pressure into a lower order space to avoid a volumetric locking. The variational formulation for multibody frictional contact is developed using a penalty method that regularizes the solution of the variational inequality. The material derivative of continuum mechanics is utilized to develop the continuum-based shape design sensitivity analysis for the hyper-elastic constitutive relation and penalized contact formulation. The sensitivity equation is solved at each converged load step using the same tangent stiffness of response analysis due to the path dependency of the sensitivity of the frictional contact problem. A very accurate and efficient sensitivity results are shown through shape optimization of a windshield wiper.

**Key words** design sensitivity analysis, multibody contact, hyper-elastic material

## 1 Introduction

In general, analysis of hyper-elastic material is difficult because of complexities involved in performing nonlinear finite element analysis of rubber components, which usually experience very large deformation. An effective numerical method, which can handle material incompressibility under large deformation, is highly desirable in analyzing rubber components. For example, the penalty method (Oden and Kikuchi 1982), selective reduced integration method (Malkas and Hughes 1978), and mixed formulations (Sussman and Bathe 1987) have been used successfully for incompressible and nearly incompressible media. Recently, Chen *et al.* (1996) proposed a pressure projection method which is a generalization of the B-bar method (Hughes 1987) for linear problems to avoid volumetric locking for nearly incompressible materials. This method projects the pressure by imposing a constraint condition between the hydrostatic pressure calculated from the displacement and the pressure obtained from the pressure interpolation functions that are in a lower-order space than the space for the displacement in a least-square sense. Using the variational principle of the pressure projection method, the finite deformation analysis for the hyper-elastic material is developed using the total Lagrangian formulation or material description. The analysis method follows the incremental procedure to obtain the linearized variational form for hyper-elastic material.

To obtain a better structural design by changing the shape of the structure, shape design sensitivity analysis (DSA) is a critical step. Haug *et al.* (1986) proved the existence of sensitivity for linear elastic structural systems and derived shape sensitivity formulation based on a continuum approach. No mathematical proof is available for the existence or uniqueness of the shape sensitivity for a nonlinear structure. Under the regularity assumption, Santos and Choi (1992) derived shape sensitivity of nonlinear elastic materials. Recently, Grindeanu *et al.* (1998) developed nonlinear shape design sensitivity formulation using the meshfree method. The design sensitivity equation is obtained by taking the material derivative of the variational equation with respect to the shape design parameters at the final converged configuration. The material description is used instead of the spatial description since both the constitutive relation and design perturbation are described in the undeformed configuration for hyper-elastic material. The design sensitivity equation depends on the nonlinear responses at the final configuration and the design velocity field at the undeformed domain. The computational effort of DSA is basically the same as solving a linear system of equation.

*Received August 8, 1999*

N.H. Kim, Y.H. Park, and K.K. Choi

Center for Computer-Aided Design and Department of Mechanical Engineering, The University of Iowa, Iowa City, IA 52242, USA
e-mail: nkim@ccad.uiowa.edu
ypark@ccad.uiowa.edu
kkchoi@ccad.uiowa.edu

This makes sensitivity computation quite efficient compared to nonlinear response analysis that requires iteration. In this paper, shape DSA is developed for Mooney-Rivlin type material that includes a nearly incompressible constraint.

Contact problems are common and important aspects of mechanical systems. Metal forming, vehicle crash, projectile penetration, various sealing designs, bushings and gear systems are only a few examples where contact occur. Recent developments in computational mechanics make it possible to solve frictional contact problems accurately and efficiently. However there are not enough practical design methods for a structural system that involves frictional contact.

DSA of a contact problem is a challenging topic. For the linear structures, Mignot (1976) and Haraux (1977) proved that the projection onto a convex set in Hilbert space is directionally differentiable. Sokolowski and Zolesio (1991) derived sensitivity formulation for variational inequality (VI). They concluded that the solution of VI is directionally differentiable, and its shape sensitivity is a solution of another VI, which is a projection onto a common convex set of tangential and orthogonal subspaces. Spivey and Tortorelli (1994) presented a sensitivity formulation of a nonlinear contact problem for beam and optimized the geometry of the rigid surface. Antunez and Kleiber (1996) derived a sensitivity formulation of a contact problem using a flow approach to analyze the rigid-plastic structure. Pollock and Noor (1996) developed a nonlinear dynamic sensitivity formulation for the explicit method by taking derivatives of the finite element matrix. Many researches in the nonlinear contact DSA are confined to non-shape sensitivity formulations.

In this paper, a continuum-based shape DSA is presented for a multibody frictional contact problem with hyper-elastic material. In Sect. 2, shape DSA is introduced using the material derivative concept. The efficiency of DSA for hyper-elastic material is discussed. In Sect. 3, as a continuation of the previous work (Choi *et al.* 1998), shape DSA of multibody frictional contact is developed using the penalty method and modified Coulomb friction model. Accuracy and efficiency of the proposed method is demonstrated in Sect. 4 through shape optimization of a windshield wiper contact problem.

## 2
## Design sensitivity analysis of hyper-elasticity

If there exists a strain energy density function such that the stress can be obtained from the derivative of the strain energy with respect to the strain, the system is path-independent. The nonlinear variational equation, however, is solved using a step-by-step incremental procedure with a number of load steps to finally reach the total equilibrium. On the other hand, the design sensitivity equation is solved at the final converged load step with the same tangent stiffness operator as response analysis. One linear system of equation is solved for each design parameter without any iteration. Thus, the cost of sensitivity computation is quite small compared to that of incremental response analysis.

### 2.1
### Response analysis of nonlinear structures with hyper-elastic materials

#### 2.1.1
#### Pressure projection method

The nearly incompressibility of the hyper-elastic material can be imposed by using a large magnitude of the bulk modulus that relates the volumetric stress and strain. For the Mooney-Rivlin type material model with the displacement-based single field formulation, the strain energy density function $W$ is defined by

$$W(J_1, J_2, J_3) = D_{10}(J_1 - 3) + D_{01}(J_2 - 3) +$$

$$\frac{K}{2}(J_3 - 1)^2 = W_1(J_1, J_2) + W_2(J_3)\,, \tag{1}$$

where $D_{10}$, $D_{01}$ are the material constants and $K$ is the bulk modulus. Also, $J_1 = I_1 I_3^{-1/3}$, $J_2 = I_2 I_3^{-2/3}$, and $J_3 = I_3^{1/2}$ are reduced invariants where $I_1$, $I_2$, and $I_3$ are invariants of the Green deformation tensor. The reason for introducing the reduced invariants is to separate the dilation part from the distortion part. Since $W_1$ contains only the distortional energy and is independent of dilation, the volumetric locking is related to $W_2$ only. The hydrostatic pressure is defined as the derivative of $W_2$

$$\tilde{p} \equiv \frac{\partial W(J_1, J_2, J_3)}{\partial J_3} = \frac{\partial W_2(J_3)}{\partial J_3} = K(J_3 - 1)\,. \tag{2}$$

Since a large magnitude of $K$ is used to impose nearly incompressibility, a numerical instability can be caused in computing the pressure in (2) from the displacement. Chen *et al.* (1996) proposed a pressure projection method to relieve this instability or volumetric locking. In this method, the pressure obtained by (2) is projected onto the lower-order space in the least square sense. That is, choose $\mathbf{p} = [p_1, p_2, \ldots, p_n]^T$ to minimize

$$\Psi(\mathbf{p}) = \left\|\tilde{p} - \mathbf{Q}^T\mathbf{p}\right\|_{L_2}^2 = \int_\Omega \left(\tilde{p} - \mathbf{Q}^T\mathbf{p}\right)^2 \mathrm{d}\Omega\,, \tag{3}$$

where $\mathbf{Q}(x) = [Q_1, Q_2, \ldots, Q_n]^T$ is a basis function for the projected space. The stationary condition of (3) is

$$\int_\Omega \overline{\mathbf{p}}^T \mathbf{Q}(\tilde{p} - \mathbf{Q}^T\mathbf{p})\,\mathrm{d}\Omega = 0\,. \tag{4}$$

The "over bar" is used to denote the first-order variation throughout this paper. The variable $\mathbf{p}$ is added to the system and (4) is the additional equations to determine $\mathbf{p}$.

The pressure projection method is used in this paper with the constant basis function $\mathbf{Q} = [1]$ that implies the constant pressure interpolation within an element, and the pressure is condensed at each element. For this choice of basis function, (4) becomes

$$\int_{\Omega} \overline{p} H \, \mathrm{d}\Omega = 0 \,, \tag{5}$$

where $H \equiv J_3 - 1 - p/K$ is the term corresponding to the volumetric strain. In the pressure projection method, (5) is added to the structural variational form.

### 2.1.2 Principle of virtual work for nonlinear structures

For the hyper-elastic material, the constitutive equation can be obtained using the strain energy density function $W$ with an independently projected pressure term. The second Piola-Kirchhoff stress tensor can be obtained by

$$\mathbf{S} = W_{,\mathbf{E}} = D_{10} J_{1,\mathbf{E}} + D_{01} J_{2,\mathbf{E}} + p J_{3,\mathbf{E}} \,, \tag{6}$$

where $\mathbf{E}$ is a Lagrangian strain tensor defined as

$$\mathbf{E} = \frac{1}{2}(\mathbf{F}^T\mathbf{F} - \mathbf{I}) \,, \tag{7}$$

and $\mathbf{F}$ and $\mathbf{I}$ are the deformation gradient and 2-nd order identity tensor, respectively. The first variation of the strain energy density function in (1) can be written as

$$\overline{W} = W_{,\mathbf{E}} : \overline{\mathbf{E}} = \mathbf{S} : \overline{\mathbf{E}} \,, \tag{8}$$

where $\overline{\mathbf{E}}$ is the variation of the Lagrangian strain defined by

$$\overline{\mathbf{E}} = \mathrm{sym}(\nabla \overline{\mathbf{z}}^T \mathbf{F}) \,, \tag{9}$$

and $\nabla = \partial/\partial\mathbf{x}$ is the gradient operator with respect to the undeformed configuration, $\mathbf{z}$ is the displacement vector, and $\mathrm{sym}(\bullet)$ denotes the symmetric part of the tensor.

The structural energy form is composed of the variation of the strain energy density function in (8) and the pressure projection term in (5). The structural energy form is defined as

$$a(\mathbf{r}, \overline{\mathbf{r}}) \equiv \int_{\Omega} \mathbf{S} : \overline{\mathbf{E}} \, \mathrm{d}\Omega + \int_{\Omega} \overline{p} H \, \mathrm{d}\Omega \,, \tag{10}$$

with a new response variable $\mathbf{r}^T \equiv [\mathbf{z}^T, p]$, which contains all unknown variables in analysis. The virtual work done by the external force is defined as

$$\ell(\overline{\mathbf{r}}) \equiv \int_{\Omega} \overline{\mathbf{z}}^T \mathbf{f}^B \, \mathrm{d}\Omega + \int_{\Gamma_T} \overline{\mathbf{z}}^T \mathbf{f}^S \, \mathrm{d}\Gamma \,, \tag{11}$$

where $\mathbf{f}^B$ is the body force vector; $\mathbf{f}^S$ is the surface traction vector; and $\Gamma_T$ is the traction boundary. The applied external force is assumed to be independent of the deformation. Note that $a(\mathbf{r}, \overline{\mathbf{r}})$ is a nonlinear form whereas, $\ell(\overline{\mathbf{r}})$ is a linear form. The principle of virtual work states that for given $\mathbf{f}^B$, $\mathbf{f}^S$, and $\zeta$, find the response variable $\mathbf{r} \in V$ such that

$$a(\mathbf{r}, \overline{\mathbf{r}}) = \ell(\overline{\mathbf{r}}) \,, \quad \forall \overline{\mathbf{r}} \in Z \,, \tag{12}$$

where $V$ is the solution space, $\zeta$ is the prescribed displacement, and $Z$ is the space of kinematically admissible displacements.

### 2.1.3 Linearization of variational equation

Since the structural energy form $a(\mathbf{r}, \overline{\mathbf{r}})$ is nonlinear, a step-by-step incremental solution procedure is used for each load step to finally reach the total applied load after a number of load steps. Let the solution at time $t_{n-1}$ be known and the solution at time $t_n$ is required. Here time is not a physical time for a quasi-static problem but denotes a discrete load step. For the finite deformation nonlinear hyper-elastic material, the governing variational equation at time $t_n$ is

$$a({}^n\mathbf{r}, \overline{\mathbf{r}}) = \ell(\overline{\mathbf{r}}) \,, \quad \forall \overline{\mathbf{r}} \in Z \,, \tag{13}$$

where the left superscript $n$ is used to denote the configuration time $t_n$ and will be omitted unless necessary for clarification. Since the configuration at $t_n$ is unknown, (13) can be solved by the Newton-Raphson iteration method using linearization. The stress can be expressed by an incremental form as

$$\Delta\mathbf{S} \cong W_{,\mathbf{E},\mathbf{E}} : \Delta\mathbf{E} + W_{,\mathbf{E},p} \Delta p = \mathbf{C} : \Delta\mathbf{E} + J_{3,\mathbf{E}} \Delta p \,, \tag{14}$$

where $\mathbf{C}$ is the 4-th order incremental stress-strain tensor at time $t_n$ referred to the configuration at time $t_0$, and $\Delta\mathbf{E} = \mathrm{sym}(\nabla \Delta\mathbf{z}^T \mathbf{F})$ and $\Delta p$ are the incremental strain and pressure, respectively.

The linearized structural energy form can be obtained using (14) as

$$a^*(\mathbf{r}; \Delta\mathbf{r}, \overline{\mathbf{r}}) \equiv \int_{\Omega} \big[ \overline{\mathbf{E}} : (\mathbf{C} : \Delta\mathbf{E} + J_{3,\mathbf{E}} \Delta p) + \mathbf{S} : \Delta\overline{\mathbf{E}} \big] \, \mathrm{d}\Omega + \int_{\Omega} \overline{p} \left( J_{3,\mathbf{E}} : \Delta\mathbf{E} - \frac{\Delta p}{K} \right) \mathrm{d}\Omega \,, \tag{15}$$

where $\Delta\overline{\mathbf{E}} = \mathrm{sym}(\nabla \overline{\mathbf{z}}^T \nabla \Delta\mathbf{z})$. Note that $a^*(\mathbf{r}; \Delta\mathbf{r}, \overline{\mathbf{r}})$ is bilinear with respect to $\Delta\mathbf{r}$ and $\overline{\mathbf{r}}$, and depends on the configuration at time $t_n$ through $\mathbf{r}$. Since the applied load is assumed to be conservative, the load form in (11) is linear and thus no linearization is required. Let the current

time be $t_n$ and the current iteration count be $k+1$, then the linearized incremental equation is

$$a^*\left({}^n\mathbf{r}^k; \Delta\mathbf{r}^{k+1}, \overline{\mathbf{r}}\right) = \ell(\overline{\mathbf{r}}) - a\left({}^n\mathbf{r}^k, \overline{\mathbf{r}}\right), \quad \forall \overline{\mathbf{r}} \in Z. \tag{16}$$

The pressure term can be condensed at an element level by directly solving terms containing the pressure variation in (15).

## 2.2 Shape design sensitivity analysis of nonlinear structures with hyper-elastic materials

### 2.2.1 Material derivatives

In shape design, the shape of the domain that a structural component occupies is treated as the design variable. Consider an undeformed domain $\Omega$ with boundary $\Gamma$ at the initial design $\tau = 0$ as shown in Fig. 1. Suppose that only one parameter $\tau$ defines the mapping $\mathbf{T}$ for shape perturbation between the original and perturbed geometries at the undeformed configuration. The mapping for shape perturbation, $\mathbf{T} : \mathbf{X} \to \mathbf{X}_\tau(\mathbf{X})$, $\mathbf{X} \in \Omega$, is given by

$$\mathbf{X}_\tau = \mathbf{T}(\mathbf{X}, \tau), \quad \Omega_\tau = \mathbf{T}(\Omega, \tau), \quad \Gamma_\tau = \mathbf{T}(\Gamma, \tau). \tag{17}$$

The mapping of (17) can be interpreted as a dynamic process perturbing a continuum shape design from an initial domain $\Omega$, at $\tau = 0$, to a perturbed domain $\Omega_\tau$. Define a design velocity field as

$$\mathbf{V}(\mathbf{X}_\tau, \tau) \equiv \frac{\mathrm{d}\mathbf{X}_\tau}{\mathrm{d}\tau} = \frac{\mathrm{d}\mathbf{T}(\mathbf{X}, \tau)}{\mathrm{d}\tau} = \frac{\partial \mathbf{T}(\mathbf{X}, \tau)}{\partial \tau}, \tag{18}$$

with $\tau$ playing the role of time. In a neighborhood of $\tau = 0$, under the reasonable regularity hypothesis and ignoring higher order terms,

$$\mathbf{T}(\mathbf{X}, \tau) = \mathbf{T}(\mathbf{X}, 0) + \tau \frac{\mathrm{d}\mathbf{T}(\mathbf{X}, 0)}{\mathrm{d}\tau} + \mathcal{O}(\tau^2) \approx$$

$$\mathbf{X} + \tau \mathbf{V}(\mathbf{X}, 0), \tag{19}$$

where $\mathbf{X} \equiv \mathbf{T}(\mathbf{X}, 0)$ and $\mathbf{V}(\mathbf{X}) \equiv \mathbf{V}(\mathbf{X}, 0)$. Detailed formulae for the material derivative can be found in Haug *et al.* (1986).

Consider the governing variational equation at $t_n$ for the perturbed shape design $\Omega_\tau$ as

$$a_{\Omega_\tau}(\mathbf{r}_\tau, \overline{\mathbf{r}}_\tau) = \ell_{\Omega_\tau}(\overline{\mathbf{r}}_\tau), \quad \forall \overline{\mathbf{r}}_\tau \in Z_\tau, \tag{20}$$

where $Z_\tau$ is the space of the kinematically admissible displacements space for the perturbed design and the subscript $\Omega_\tau$ indicates the dependence of these terms on the shape of the domain.

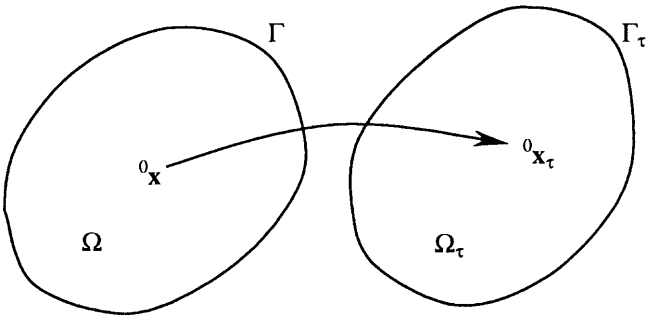


**Fig. 1** Variation of undeformed domain by one-parameter family of mappings

The solution $\mathbf{r}_\tau(\mathbf{X}_\tau)$ of (20) referred to the initial coordinates $\mathbf{X}_\tau$ of the perturbed domain is assumed to be differentiable with respect to the shape design variable. The pointwise material derivative of $\mathbf{r}_\tau(\mathbf{X}_\tau)$ at $\mathbf{X} \in \Omega$ is defined as

$$\dot{\mathbf{r}} \equiv \frac{\mathrm{d}}{\mathrm{d}\tau}\mathbf{r}_\tau\left[\mathbf{X} + \tau \mathbf{V}(\mathbf{X})\right]|_{\tau=0} =$$

$$\lim_{\tau \to 0} \frac{\mathbf{r}_\tau\left[\mathbf{X} + \tau \mathbf{V}(\mathbf{X})\right] - \mathbf{r}(\mathbf{X})}{\tau}. \tag{21}$$

### 2.2.2 Nonlinear shape design sensitivity analysis with hyper-elastic materials

Consider the structural energy form at $\Omega_\tau$,

$$a_{\Omega_\tau}(\mathbf{r}_\tau, \overline{\mathbf{r}}_\tau) \equiv \int_{\Omega_\tau} \left(\mathbf{S}_\tau : \overline{\mathbf{E}}_\tau + \overline{p}_\tau H_\tau\right) \mathrm{d}\Omega. \tag{22}$$

The 2-nd Piola-Kirchhoff stress sensitivity can be obtained by taking derivative of (6) with respect to the displacement and pressure,

$$\frac{\mathrm{d}}{\mathrm{d}\tau}(\mathbf{S}) = \mathbf{C} : \frac{\mathrm{d}}{\mathrm{d}\tau}(\mathbf{E}) + J_{3,\mathbf{E}} \frac{\mathrm{d}}{\mathrm{d}\tau}(p). \tag{23}$$

Since the Lagrangian strain tensor is defined by the deformation gradient, the design derivative of $\mathbf{F}$ is derived first as

$$\frac{\mathrm{d}}{\mathrm{d}\tau}(\mathbf{F}) = \frac{\mathrm{d}}{\mathrm{d}\tau}(\mathbf{I} + \nabla \mathbf{z}) = \nabla \dot{\mathbf{z}} - \nabla \mathbf{z} \nabla \mathbf{V}. \tag{24}$$

Thus, the material derivative of the Lagrangian strain tensor in (7) can be expressed as

$$\frac{\mathrm{d}}{\mathrm{d}\tau}(\mathbf{E}) = \Delta \mathbf{E}(\dot{\mathbf{z}}) + \mathbf{E}_V(\mathbf{z}), \tag{25}$$

where $\mathbf{E}_V(\mathbf{z})$ represents terms depending on the response analysis result and design velocity field. If the response analysis result is known then $\mathbf{E}_V(\mathbf{z})$ can be obtained as

$$\mathbf{E}_V(\mathbf{z}) = -\text{sym}\left[(\nabla\mathbf{z}\nabla\mathbf{V})^T\mathbf{F}\right] . \tag{26}$$

The material derivative of the Lagrangian strain variation can be derived from (9) as

$$\frac{\mathrm{d}}{\mathrm{d}\tau}(\overline{\mathbf{E}}) = \Delta\overline{\mathbf{E}}(\dot{\mathbf{z}},\overline{\mathbf{z}}) + \overline{\mathbf{E}}_V(\mathbf{z},\overline{\mathbf{z}}) , \tag{27}$$

where from the response analysis result and design velocity field, $\overline{\mathbf{E}}_V(\mathbf{z},\overline{\mathbf{z}})$ can be obtained using

$$\overline{\mathbf{E}}_V(\mathbf{z},\overline{\mathbf{z}}) = -\text{sym}\left[(\nabla\overline{\mathbf{z}}\nabla\mathbf{V})^T\mathbf{F}\right] - \text{sym}\left[\nabla\overline{\mathbf{z}}^T(\nabla\mathbf{z}\nabla\mathbf{V})\right] . \tag{28}$$

Evaluation of the second integrand of (22) is straightforward.

By using relations in (23) through (28), the material derivative of the structural energy form becomes

$$\frac{\mathrm{d}}{\mathrm{d}\tau}\left[a_\Omega(\mathbf{r},\overline{\mathbf{r}})\right] = a^*_\Omega(\mathbf{r};\dot{\mathbf{r}},\overline{\mathbf{r}}) + a'_V(\mathbf{r},\overline{\mathbf{r}}) , \tag{29}$$

where

$$a'_V(\mathbf{r},\overline{\mathbf{r}}) \equiv \int_\Omega \Big[\overline{\mathbf{E}} : \mathbf{C} : \mathbf{E}_V + \mathbf{S} : \overline{\mathbf{E}}_V + \overline{p}J_{3,\mathbf{E}} : \mathbf{E}_V +$$

$$(\mathbf{S} : \overline{\mathbf{E}} + \overline{p}H)\text{div}\,\mathbf{V}\Big]\,\mathrm{d}\Omega , \tag{30}$$

is the structural fictitious load form, which explicitly depends on the design velocity fields and the solution at time $t_n$. If a converged solution is obtained at $t_n$, then (30) can be computed using the given design velocity field $\mathbf{V}$. The expression $a^*_\Omega(\mathbf{r};\dot{\mathbf{r}},\overline{\mathbf{r}})$ in (29) is the same form as in (15) if $\Delta\mathbf{r}$ is substituted into $\dot{\mathbf{r}}$.

The load linear form defined in (11) can be perturbed the same way as the structural energy form. For the perturbed domain $\Omega_\tau$, the load linear form is

$$\ell_{\Omega_\tau}(\overline{\mathbf{r}}_\tau) = \int_{\Omega_\tau} \overline{\mathbf{z}}_\tau^T\mathbf{f}_\tau^B\,\mathrm{d}\Omega + \int_{\Gamma_{T_\tau}} \overline{\mathbf{z}}_\tau^T\mathbf{f}_\tau^S\,\mathrm{d}\Gamma , \tag{31}$$

and the material derivative is $\mathrm{d}\ell_\Omega(\overline{\mathbf{r}})/\,\mathrm{d}\tau = \ell'_V(\overline{\mathbf{r}})$ where the fictitious load due to the external force is

$$\ell'_V(\overline{\mathbf{r}}) = \int_\Omega \left[\overline{\mathbf{z}}^T(\nabla\mathbf{f}^{B^T}\mathbf{V}) + \overline{\mathbf{z}}^T\mathbf{f}^B\text{div}\,\mathbf{V}\right]\,\mathrm{d}\Omega +$$

$$\int_{\Gamma_T} \left[\overline{\mathbf{z}}^T(\nabla\mathbf{f}^{S^T}\mathbf{V}) + \kappa\overline{\mathbf{z}}^T\mathbf{f}^S(\mathbf{V}^T\mathbf{n})\right]\,\mathrm{d}\Gamma . \tag{32}$$

Here it is assumed that the external force is independent of the design change. By combining (29) and (32), the material derivative of the variational equation for the hyper-elastic material is obtained as

$$a^*_\Omega({}^n\mathbf{r};{}^n\dot{\mathbf{r}},\overline{\mathbf{r}}) = \ell'_V(\overline{\mathbf{r}}) - a'_V({}^n\mathbf{r},\overline{\mathbf{r}}) , \quad \forall\overline{\mathbf{r}} \in Z , \tag{33}$$

which can be solved using the already decomposed tangent stiffness matrix at the converged configuration with a different fictitious load for each shape design parameter.Even though analysis requires an iterative method to converge at $t_n$, the linear sensitivity equation (33) is solved without iteration using the tangent stiffness matrix at $t_n$, which is the converged configuration. Since the left side of (33) is already decomposed from analysis, it is quite efficient to solve the linear system of sensitivity equations.

## 3 Design sensitivity analysis of multibody frictional contact problem

### 3.1 Response analysis of contact problem

Unlike a flexible-rigid body contact case (Choi *et al.* 1998), for the multibody contact (or flexible-flexible body contact) problem, the contact point depends on the motion of a slave body and a master body together since the second body also moves as it deforms. The normal contact condition prevents penetration of one body into another and the tangential slip represents frictional behaviour of the contact surface. A regularized Coulomb friction law proposed by Wriggers *et al.* (1990) is utilized in this paper.

#### 3.1.1 Contact condition

Figure 2 shows a general contact condition between two bodies in $\mathbf{R}^2$. Body 1 is referred to as the slave body and body 2 as the master body. The surface coordinate of the master body $\mathbf{x}_c \in \Gamma_c^2$ can be represented by a natural coordinate $\xi$ along the master surface. As the point $\mathbf{x} \in \Gamma_c^1$ on the slave surface is in contact with the point $\mathbf{x}_c \in \Gamma_c^2$ on the master surface, $\mathbf{x}_c$ can be represented using the natural coordinate $\xi_c$ at the contact point as $\mathbf{x}_c(\xi_c)$. The contact point moves as the slave body is deformed by the change of $\xi_c$ in addition to the deformation of the master body. The tangential vector at $\mathbf{x}_c(\xi_c)$ along the master surface can be obtained by $\mathbf{t}(\xi_c) = \mathbf{x}_{c,\xi}$ where comma represents the partial derivative.

The normal contact condition can be imposed on the structure by measuring the distance between parts of the boundaries $\Gamma_c^1$ and $\Gamma_c^2$. The impenetration condition can

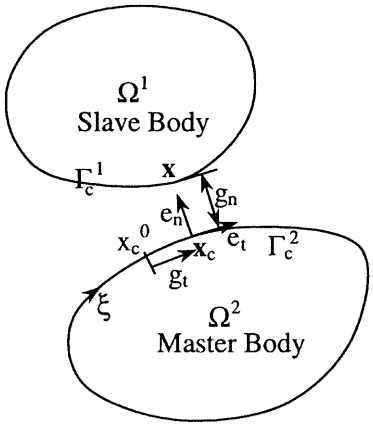


**Fig. 2** Multibody contact condition

be defined, using the normal gap function $g_n$ which measures the normal distance, as

$$g_n \equiv [\mathbf{x} - \mathbf{x}_c(\xi_c)]^T \mathbf{e}_n(\xi_c) \geq 0\,, \quad \mathbf{x} \in \Gamma_c^1\,, \quad \mathbf{x}_c \in \Gamma_c^2\,, \tag{34}$$

where $\mathbf{e}_n(\xi_c) = \mathbf{e}_3 \times \mathbf{e}_t$ is the unit outward normal vector of the master surface at the contact point, $\mathbf{e}_t = \mathbf{t}/\|\mathbf{t}\|$ is the unit tangential vector, and $\mathbf{e}_3$ is the unit vector out of plane direction fixed in $\mathbf{R}^2$.The contact point $\mathbf{x}_c \in \Gamma_c^2$ corresponding to the slave surface point $\mathbf{x} \in \Gamma_c^1$ is determined by solving the following contact consistency condition

$$\varphi(\xi_c) = [\mathbf{x} - \mathbf{x}_c(\xi_c)]^T \mathbf{e}_t(\xi_c) = 0\,. \tag{35}$$

Note that, in (35), $\mathbf{x}_c(\xi_c)$ is the closest projection point of $\mathbf{x} \in \Gamma_c^1$ onto the master surface. As the contact point moves along the master surface, a frictional force that resists the tangential relative movement exists along the tangential direction of the surface of the master body. The tangential slip function $g_t$ is the measure of the relative movement of the contact point along the master surface as

$$g_t \equiv \|\mathbf{t}^0\|(\xi_c - \xi_c^0)\,, \tag{36}$$

where $\mathbf{t}^0$ and $\xi_c^0$ are the tangential vector and natural coordinate of the previous converged time step, respectively.

If there exists a region $\Gamma_c$ which violates the impenetration conditions of (34), it is penalized by the penalty function. Similarly, the tangential movement of (36) can also be penalized. Define the contact penalty function for the violated region by

$$P = \frac{1}{2}\omega_n \int_{\Gamma_c} g_n^2 \,\mathrm{d}\Gamma + \frac{1}{2}\omega_t \int_{\Gamma_c} g_t^2 \,\mathrm{d}\Gamma\,, \tag{37}$$

where $\omega_n$ and $\omega_t$ are the penalty parameters for normal contact and tangential slip, respectively. To combine with the structural variational equation, the first-order variation of $P$, which is the contact variational form, is obtained as

$$b(\mathbf{z}, \overline{\mathbf{z}}) \equiv \overline{P} = \omega_n \int_{\Gamma_c} g_n \overline{g}_n \,\mathrm{d}\Gamma + \omega_t \int_{\Gamma_c} g_t \overline{g}_t \,\mathrm{d}\Gamma\,, \tag{38}$$

where $\omega_n g_n$ and $\omega_t g_t$ correspond to the compressive normal force and tangential traction force, respectively.

For the variational equation, the contact variational form in (38) needs to be expressed in terms of the displacement variation. For the convenience of the derivations to follow, define several scalar symbols

$$\alpha \equiv \mathbf{e}_n^T \mathbf{x}_{c,\xi\xi}\,, \quad \beta \equiv \mathbf{e}_t^T \mathbf{x}_{c,\xi\xi}\,, \quad \gamma \equiv \mathbf{e}_n^T \mathbf{x}_{c,\xi\xi\xi}\,,$$

$$c \equiv \|\mathbf{t}\|^2 - g_n \alpha\,, \quad v \equiv \|\mathbf{t}\|\|\mathbf{t}^0\| c\,. \tag{39}$$

The variations of the normal gap and tangential slip functions can be obtained by considering the variation of the contact consistency condition in (35) as

$$\overline{g}_n(\mathbf{z}; \overline{\mathbf{z}}) = (\overline{\mathbf{z}} - \overline{\mathbf{z}}_c)^T \mathbf{e}_n = \hat{\overline{\mathbf{z}}}^T \mathbf{e}_n\,, \tag{40}$$

$$\overline{g}_t = \|\mathbf{t}^0\|\overline{\xi}_c = v\hat{\overline{\mathbf{z}}}^T \mathbf{e}_t + \frac{g_n \|\mathbf{t}^0\|}{c} \overline{\mathbf{z}}_{c,\xi}^T \mathbf{e}_n\,, \tag{41}$$

where $\hat{\mathbf{z}} = \mathbf{z} - \mathbf{z}_c$ is the relative displacement between the slave and master contact points.

Using (40) and (41), the contact variational form (38) can be rewritten in terms of the variation of the displacement as

$$b(\mathbf{r}, \overline{\mathbf{r}}) = b_N(\mathbf{r}, \overline{\mathbf{r}}) + b_T(\mathbf{r}, \overline{\mathbf{r}})\,, \tag{42}$$

where

$$b_N(\mathbf{r}, \overline{\mathbf{r}}) = \omega_n \int_{\Gamma_c} g_n \hat{\overline{\mathbf{z}}}^T \mathbf{e}_n \,\mathrm{d}\Gamma\,, \tag{43}$$

$$b_T(\mathbf{r}, \overline{\mathbf{r}}) = \omega_t \int_{\Gamma_c} g_t \left( v\hat{\overline{\mathbf{z}}}^T \mathbf{e}_t + \frac{g_n \|\mathbf{t}^0\|}{c} \overline{\mathbf{z}}_{c,\xi}^T \mathbf{e}_n \right) \mathrm{d}\Gamma\,, \tag{44}$$

are the normal contact and tangential slip variational form, respectively. Note that the frictional effect in (44) also acts in the normal direction by the displacement variation of the master surface. Figure 3 shows a friction curve used in this paper. The stick condition occurs when the frictional traction force generated by the tangential slip and the penalty parameter is less than the normal force multiplied by the frictional coefficient

$$|\omega_t g_t| \leq |\mu \omega_n g_n|\,. \tag{45}$$

Otherwise, it becomes a slip condition. In (45), $\mu$ is the Coulomb friction coefficient. For the case of the slip con-

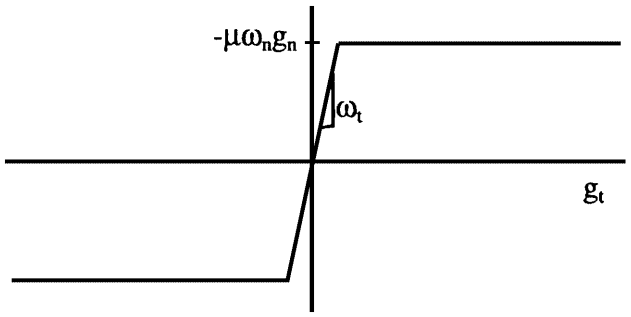


**Fig. 3** Frictional interface model

dition, the tangential slip variational form (44) is written as

$$b_T(\mathbf{r},\overline{\mathbf{r}}) = -\mu\omega_n \mathrm{sgn}(g_t) \int_{\Gamma_c} g_n \left( v\hat{\overline{\mathbf{z}}}^T \mathbf{e}_t + \frac{g_n \|\mathbf{t}^0\|}{c} \overline{\mathbf{z}}_{c,\xi}^T \mathbf{e}_n \right) \mathrm{d}\Gamma \,. \tag{46}$$

### 3.1.2 Linearization of stick condition

The nonlinear contact variational form in (42) is linearized for the Newton-Raphson iteration. The incremental forms of the normal gap and tangential slip functions can be computed using the similar procedures as obtaining the first-order variations in (40) and (41),

$$\Delta g_n(\mathbf{z};\Delta\mathbf{z}) = \mathbf{e}_n^T \Delta\hat{\mathbf{z}} \,, \tag{47}$$

$$\Delta g_t(\mathbf{z};\Delta\mathbf{z}) = v\mathbf{e}_t^T \Delta\hat{\mathbf{z}} + \left( \frac{g_n \|\mathbf{t}^0\|}{c} \right) \mathbf{e}_n^T \Delta\mathbf{z}_{c,\xi} \,, \tag{48}$$

and the incremental forms of the unit normal and tangential vectors can be derived as

$$\Delta\mathbf{e}_t = \left( \frac{\alpha \mathbf{e}_t^T \Delta\hat{\mathbf{z}}}{c} + \frac{\|\mathbf{t}\| \mathbf{e}_n^T \Delta\mathbf{z}_{c,\xi}}{c} \right) \mathbf{e}_n \,,$$

$$\Delta\mathbf{e}_n(\xi_c) = \mathbf{e}_3 \times \Delta\mathbf{e}_t \,. \tag{49}$$

Using the linearization process, the normal contact bilinear form is obtained as

$$b_N^*(\mathbf{r};\Delta\mathbf{r},\overline{\mathbf{r}}) \equiv \omega_n \int_{\Gamma_c} \left( \hat{\overline{\mathbf{z}}}^T \mathbf{e}_n \mathbf{e}_n^T \Delta\hat{\mathbf{z}} - \frac{\alpha g_n}{c} \hat{\overline{\mathbf{z}}}^T \mathbf{e}_t \mathbf{e}_t^T \Delta\hat{\mathbf{z}} \right) \mathrm{d}\Gamma -$$

$$\omega_n \int_{\Gamma_c} \frac{g_n \|\mathbf{t}\|}{c} \left( \hat{\overline{\mathbf{z}}}^T \mathbf{e}_t \mathbf{e}_n^T \Delta\mathbf{z}_{c,\xi} + \overline{\mathbf{z}}_{c,\xi}^T \mathbf{e}_n \mathbf{e}_t^T \Delta\hat{\mathbf{z}} \right) \mathrm{d}\Gamma -$$

$$\omega_n \int_{\Gamma_c} \frac{g_n^2}{c} \overline{\mathbf{z}}_{c,\xi}^T \mathbf{e}_n \mathbf{e}_n^T \Delta\mathbf{z}_{c,\xi} \, \mathrm{d}\Gamma \,. \tag{50}$$

Using the similar procedure of linearization as in the normal contact variational form, the tangential stick bilinear form can be obtained as

$$b_T^*(\mathbf{r};\Delta\mathbf{r},\overline{\mathbf{r}}) \equiv \omega_t \int_{\Gamma_c} \left\{ v^2 + \frac{v g_t}{c^2} \times \right.$$

$$\left. \left[ (\gamma\|\mathbf{t}\| - 2\alpha\beta) g_n - \beta\|\mathbf{t}\|^2 \right] \right\} \hat{\overline{\mathbf{z}}}^T \mathbf{e}_t \mathbf{e}_t^T \Delta\hat{\mathbf{z}} \, \mathrm{d}\Gamma +$$

$$\omega_t \int_{\Gamma_c} \|\mathbf{t}^0\| g_n \left( \frac{v}{c} - g_t \frac{2\beta\|\mathbf{t}\|^2 + \alpha\beta g_n - \gamma g_n \|\mathbf{t}\|}{c^3} \right) \times$$

$$\left( \hat{\overline{\mathbf{z}}}^T \mathbf{e}_t \mathbf{e}_n^T \Delta\mathbf{z}_{c,\xi} + \overline{\mathbf{z}}_{c,\xi}^T \mathbf{e}_n \mathbf{e}_t^T \Delta\hat{\mathbf{z}} \right) \mathrm{d}\Gamma +$$

$$\omega_t \int_{\Gamma_c} \frac{\alpha v g_t}{c} \hat{\overline{\mathbf{z}}}^T \left( \mathbf{e}_n \mathbf{e}_t^T + \mathbf{e}_t \mathbf{e}_n^T \right) \Delta\hat{\mathbf{z}} \, \mathrm{d}\Gamma +$$

$$\omega_t \int_{\Gamma_c} \frac{v g_t \|\mathbf{t}\|}{c} \left( \hat{\overline{\mathbf{z}}}^T \mathbf{e}_n \mathbf{e}_n^T \Delta\mathbf{z}_{c,\xi} + \overline{\mathbf{z}}_{c,\xi}^T \mathbf{e}_n \mathbf{e}_n^T \Delta\hat{\mathbf{z}} \right) \mathrm{d}\Gamma +$$

$$\omega_t \int_{\Gamma_c} g_t \frac{\|\mathbf{t}^0\| - 2v\|\mathbf{t}\|}{c} \times$$

$$\left( \hat{\overline{\mathbf{z}}}^T \mathbf{e}_n \mathbf{e}_n^T \Delta\mathbf{z}_{c,\xi} + \overline{\mathbf{z}}_{c,\xi}^T \mathbf{e}_n \mathbf{e}_n^T \Delta\hat{\mathbf{z}} \right) \mathrm{d}\Gamma +$$

$$\omega_t \int_{\Gamma_c} \left[ \left( \frac{g_n \|\mathbf{t}^0\|}{c} \right)^2 - \frac{g_n g_t \|\mathbf{t}^0\|}{c^3} \left( 3\beta g_n \|\mathbf{t}\| - \gamma g_n^2 \right) \right] \times$$

$$\overline{\mathbf{z}}_{c,\xi}^T \mathbf{e}_n \mathbf{e}_n^T \Delta\mathbf{z}_{c,\xi} \, \mathrm{d}\Gamma -$$

$$\omega_t \int_{\Gamma_c} \frac{2 g_n g_t v}{c} \overline{\mathbf{z}}_{c,\xi}^T \left( \mathbf{e}_n \mathbf{e}_t^T + \mathbf{e}_t \mathbf{e}_n^T \right) \Delta\mathbf{z}_{c,\xi} \, \mathrm{d}\Gamma +$$

$$\omega_t \int_{\Gamma_c} \frac{g_n g_t v}{c} \left( \hat{\overline{\mathbf{z}}}^T \mathbf{e}_t \mathbf{e}_n^T \Delta\mathbf{z}_{c,\xi\xi} + \overline{\mathbf{z}}_{c,\xi\xi}^T \mathbf{e}_n \mathbf{e}_t^T \Delta\hat{\mathbf{z}} \right) \mathrm{d}\Gamma +$$

$$\omega_t \int_{\Gamma_c} \frac{g_n^2 g_t \|\mathbf{t}^0\|}{c^2} \left( \overline{\mathbf{z}}_{c,\xi}^T \mathbf{e}_n \mathbf{e}_n^T \Delta\mathbf{z}_{c,\xi\xi} + \overline{\mathbf{z}}_{c,\xi\xi}^T \mathbf{e}_n \mathbf{e}_n^T \Delta\mathbf{z}_{c,\xi} \right) \mathrm{d}\Gamma \,. \tag{51}$$

From (50) and (51), the linearized contact form can be written as

$$b^*(\mathbf{r};\Delta\mathbf{r},\overline{\mathbf{r}}) = b_N^*(\mathbf{r};\Delta\mathbf{r},\overline{\mathbf{r}}) + b_T^*(\mathbf{r};\Delta\mathbf{r},\overline{\mathbf{r}}) \,. \tag{52}$$

Note that the contact bilinear form in (52) for the stick condition is symmetric with respect to $\Delta\mathbf{z}$ and $\overline{\mathbf{z}}$.

### 3.1.3
### Linearization of slip condition

For the slip contact condition, (46) is used for tangential slip. The normal contact variational form $b_N(\mathbf{r},\overline{\mathbf{r}})$ in (43) has the same form as in the stick condition and its linearized form $b_n^*(\mathbf{r};\Delta\mathbf{r},\overline{\mathbf{r}})$ is given in (50). Using the relationship $\omega_t = -\mu\omega_n \mathrm{sgn}(g_t)$ for the case of the slip contact, the linearization of (46) leads to the tangential slip bilinear form as

$$
\begin{aligned}
b_T^*(\mathbf{r};\Delta\mathbf{r},\overline{\mathbf{r}}) \equiv\ & \omega_t \int_{\Gamma_c} v\hat{\overline{\mathbf{z}}}^T \mathbf{e}_t\mathbf{e}_n^T \Delta\hat{\mathbf{z}}\,\mathrm{d}\Gamma + \\
& \omega_t \int_{\Gamma_c} \frac{vg_n}{c^2}\left[\Big(\gamma\|\mathbf{t}\| - 2\alpha\beta\Big)g_n - \beta\|\mathbf{t}\|^2\right]\hat{\overline{\mathbf{z}}}^T \mathbf{e}_t\mathbf{e}_t^T \Delta\hat{\mathbf{z}}\,\mathrm{d}\Gamma - \\
& \omega_t \int_{\Gamma_c} \|\mathbf{t}^0\| g_n^2 \frac{2\beta\|\mathbf{t}\|^2 + \alpha\beta g_n - \gamma g_n\|\mathbf{t}\|}{c^3} \times \\
& \Big(\hat{\overline{\mathbf{z}}}^T \mathbf{e}_t\mathbf{e}_n^T \Delta\mathbf{z}_{c,\xi} + \overline{\mathbf{z}}_{c,\xi}^T \mathbf{e}_n\mathbf{e}_t^T \Delta\hat{\mathbf{z}}\Big)\,\mathrm{d}\Gamma + \\
& \omega_t \int_{\Gamma_c} \frac{\alpha v g_n}{c}\hat{\overline{\mathbf{z}}}^T \left(\mathbf{e}_n\mathbf{e}_t^T + \mathbf{e}_t\mathbf{e}_n^T\right)\Delta\hat{\mathbf{z}}\,\mathrm{d}\Gamma + \\
& \omega_t \int_{\Gamma_c} \frac{vg_n\|\mathbf{t}\|}{c}\hat{\overline{\mathbf{z}}}^T \mathbf{e}_n\mathbf{e}_n^T \Delta\mathbf{z}_{c,\xi}\,\mathrm{d}\Gamma + \\
& \omega_t \int_{\Gamma_c} g_n \frac{v\|\mathbf{t}\| + \|\mathbf{t}^0\|}{c}\overline{\mathbf{z}}_{c,\xi}^T \mathbf{e}_n\mathbf{e}_n^T \Delta\hat{\mathbf{z}}\,\mathrm{d}\Gamma + \\
& \omega_t \int_{\Gamma_c} g_n \frac{\|\mathbf{t}^0\| - 2v\|\mathbf{t}\|}{c} \times \\
& \Big(\hat{\overline{\mathbf{z}}}^T \mathbf{e}_n\mathbf{e}_n^T \Delta\mathbf{z}_{c,\xi} + \overline{\mathbf{z}}_{c,\xi}^T \mathbf{e}_n\mathbf{e}_n^T \Delta\hat{\mathbf{z}}\Big)\,\mathrm{d}\Gamma - \\
& \omega_t \int_{\Gamma_c} \frac{g_n^2\|\mathbf{t}^0\|}{c^3}\left(3\beta g_n\|\mathbf{t}\| - \gamma g_n^2\right)\overline{\mathbf{z}}_{c,\xi}^T \mathbf{e}_n\mathbf{e}_n^T \Delta\mathbf{z}_{c,\xi}\,\mathrm{d}\Gamma - \\
& \omega_t \int_{\Gamma_c} \frac{2g_n^2 v}{c}\overline{\mathbf{z}}_{c,\xi}^T \left(\mathbf{e}_n\mathbf{e}_t^T + \mathbf{e}_t\mathbf{e}_n^T\right)\Delta\mathbf{z}_{c,\xi}\,\mathrm{d}\Gamma + \\
& \omega_t \int_{\Gamma_c} \frac{g_n^2 v}{c}\Big(\hat{\overline{\mathbf{z}}}^T \mathbf{e}_t\mathbf{e}_n^T \Delta\mathbf{z}_{c,\xi\xi} + \overline{\mathbf{z}}_{c,\xi\xi}^T \mathbf{e}_n\mathbf{e}_t^T \Delta\hat{\mathbf{z}}\Big)\,\mathrm{d}\Gamma + \\
& \omega_t \int_{\Gamma_c} \frac{g_n^3\|\mathbf{t}^0\|}{c^2}\left(\overline{\mathbf{z}}_{c,\xi}^T \mathbf{e}_n\mathbf{e}_n^T \Delta\mathbf{z}_{c,\xi\xi} + \overline{\mathbf{z}}_{c,\xi\xi}^T \mathbf{e}_n\mathbf{e}_n^T \Delta\mathbf{z}_{c,\xi}\right)\mathrm{d}\Gamma\,.
\end{aligned}
\tag{53}
$$

Then, the linearized contact form in (52) is applicable where (53) is used for $b_T^*(\mathbf{r};\Delta\mathbf{r},\overline{\mathbf{r}})$. Unlike the stick contact, in the case of the slip contact, the contact bilinear form in (52) is not symmetric. The system is not conservative as the frictional slip dissipates energy.

### 3.1.4
### Variational principle for finite deformation with frictional contact problem

The principle of virtual work with contact constraint can be written as

$$
a(\mathbf{r},\overline{\mathbf{r}}) + b(\mathbf{r},\overline{\mathbf{r}}) = \ell(\overline{\mathbf{r}})\,, \quad \forall\overline{\mathbf{r}} \in Z\,. \tag{54}
$$

Let the current configuration be $t_n$ and $k$ is the last iteration counter. Assuming that the external force is independent of the displacement, the linearized incremental equation of (54) is obtained as

$$
\begin{aligned}
& a^*({}^n\mathbf{r}^k;\Delta\mathbf{r}^{k+1},\overline{\mathbf{r}}) + b^*({}^n\mathbf{r}^k;\Delta\mathbf{r}^{k+1},\overline{\mathbf{r}}) = \\
& \ell(\overline{\mathbf{r}}) - a({}^n\mathbf{r}^k,\overline{\mathbf{r}}) - b({}^n\mathbf{r}^k,\overline{\mathbf{r}})\,, \quad \forall\overline{\mathbf{r}} \in Z\,,
\end{aligned}
\tag{55}
$$

which is linear in incremental displacement for a given displacement variation. The linearized system (55) is solved iteratively for the incremental displacement until the residual forces [right side of (55)] become zero at each load step. The path dependency of the problem comes from the tangential slip function.

## 3.2
## Design sensitivity analysis of frictional contact problem

Consider the governing variational equation at $t_n$ for the perturbed shape design $\Omega_\tau$ as

$$
a_{\Omega_\tau}(\mathbf{r}_\tau,\overline{\mathbf{r}}_\tau) + b_{\Gamma_{C\tau}}(\mathbf{r}_\tau,\overline{\mathbf{r}}_\tau) = \ell_{\Omega_\tau}(\overline{\mathbf{r}}_\tau)\,, \quad \forall\overline{\mathbf{r}}_\tau \in Z_\tau\,. \tag{56}
$$

The material derivative of a structural energy form and external load form in (56) for the hyper-elastic material was derived in (33).

The contact point on the master surface can be perturbed by changing the natural coordinate corresponding to the contact point in the tangential direction as

$$
\frac{\mathrm{d}}{\mathrm{d}\tau}(\mathbf{x}_c) = \mathbf{V}_c + \dot{\mathbf{z}}_c + \mathbf{t}\frac{\mathrm{d}}{\mathrm{d}\tau}(\xi_c)\,. \tag{57}
$$

Since the normal contact variational form appears in both the stick and slip conditions, the material derivative of the normal contact variational form is considered first. A normal contact variational form at the perturbed domain is

$$
b_{N_\tau}(\mathbf{r}_\tau,\overline{\mathbf{r}_\tau}) = \omega_n \int_{\Gamma_{C\tau}} g_{n\tau}\hat{\overline{\mathbf{z}}}_\tau^T \mathbf{e}_{n\tau}\,\mathrm{d}\Gamma\,. \tag{58}
$$

The derivatives of the unit normal vector and the normal gap function in (58) depend on the derivative of the natural coordinate at the contact point, which can be obtained from the variation of the contact consistency condition in (35) as

$$
\frac{\mathrm{d}}{\mathrm{d}\tau}(\xi_c) = \frac{\|\mathbf{t}\|}{c}\mathbf{e}_t^T\left(\hat{\mathbf{V}} + \hat{\dot{\mathbf{z}}}\right) + \frac{g_n}{c}\mathbf{e}_n^T\left(\mathbf{V}_{c,\xi} + \dot{\mathbf{z}}_{c,\xi}\right)\,, \tag{59}
$$

where $\hat{\mathbf{V}} = \mathbf{V} - \mathbf{V}_c$ and $\hat{\dot{\mathbf{z}}} = \dot{\mathbf{z}} - \dot{\mathbf{z}}_c$. The material derivatives of the unit normal vector and the tangential vector can be expressed in terms of design velocity and material derivative of the displacement as

$$\frac{\mathrm{d}}{\mathrm{d}\tau}(\mathbf{e}_t) = \left[\frac{\alpha}{c}\mathbf{e}_t^T\left(\hat{\mathbf{V}} + \hat{\dot{\mathbf{z}}}\right) + \frac{\|\mathbf{t}\|}{c}\mathbf{e}_n^T\left(\mathbf{V}_{c,\xi} + \dot{\mathbf{z}}_{c,\xi}\right)\right]\mathbf{e}_n\,, \tag{60}$$

and $\mathrm{d}/\,\mathrm{d}\tau(\mathbf{e}_t) = \mathbf{e}_3 \times \mathrm{d}/\,\mathrm{d}\tau(\mathbf{e}_t)$. The material derivative of the normal gap function can be found by taking the derivative of (34) and considering (59) as

$$\frac{\mathrm{d}}{\mathrm{d}\tau}(g_n) = \left(\hat{\mathbf{V}} + \hat{\dot{\mathbf{z}}}\right)^T\mathbf{e}_n\,. \tag{61}$$

Using (60) and (61), the derivative of the normal contact variational form in (58) at the perturbed boundary $\Gamma_\tau$ can be obtained as

$$\frac{\mathrm{d}}{\mathrm{d}\tau}b_N(\mathbf{r},\overline{\mathbf{r}}) = b_N^*(\mathbf{r};\dot{\mathbf{r}},\overline{\mathbf{r}}) + b_N'(\mathbf{r},\overline{\mathbf{r}})\,, \tag{62}$$

where $b_N^*(\mathbf{r};\dot{\mathbf{r}},\overline{\mathbf{r}})$ is the same form as in (50) by substituting $\Delta\mathbf{r}$ into $\dot{\mathbf{r}}$ and $b_N'(\mathbf{r},\overline{\mathbf{r}})$ is the normal contact fictitious load form

$$b_N'(\mathbf{r},\overline{\mathbf{r}}) = b_N^*(\mathbf{r};\mathbf{V},\overline{\mathbf{r}}) + \omega_n\int_{\Gamma_c}\kappa g_n\hat{\overline{\mathbf{z}}}^T\mathbf{e}_n(\mathbf{V}^T\mathbf{n})\,\mathrm{d}\Gamma\,, \tag{63}$$

which depends explicitly on the design velocity field.

### 3.2.1 DSA formulation for stick condition

Before taking the material derivative of the tangential slip function in (36), the material derivatives of $\xi_c^0$ and $\|\mathbf{t}^0\|$ are computed first using the relation (59) at load step $t_{n-1}$ as

$$\frac{\mathrm{d}}{\mathrm{d}\tau}\xi_c^0 = \frac{\|\mathbf{t}^0\|}{c^0}\mathbf{e}_t^{0^T}\left(\hat{\mathbf{V}} + \hat{\dot{\mathbf{z}}}^0\right) + \frac{g_n^0}{c^0}\mathbf{e}_n^{0^T}\left(\mathbf{V}_{c,\xi} + \dot{\mathbf{z}}_{c,\xi}^0\right)\,, \tag{64}$$

$$\frac{\mathrm{d}}{\mathrm{d}\tau}\|\mathbf{t}^0\| = \mathbf{e}_t^{0^T}\left(\mathbf{V}_{c,\xi} + \dot{\mathbf{z}}_{c,\xi}^0\right) + \frac{\beta^0\|\mathbf{t}^0\|}{c^0}\mathbf{e}_t^{0^T}\left(\hat{\mathbf{V}} + \hat{\dot{\mathbf{z}}}^0\right) +$$

$$\frac{\beta^0 g_n^0}{c^0}\mathbf{e}_n^{0^T}\left(\mathbf{V}_{c,\xi} + \dot{\mathbf{z}}_{c,\xi}^0\right)\,, \tag{65}$$

where $\dot{\mathbf{z}}^0$ is the material derivative of the displacement at load step $t_{n-1}$. Even though all the quantities are evaluated at time $t_{n-1}$, the design velocity is evaluated at the undeformed configuration because the design perturbation occurs at ${}^0\Omega$. The material derivative of tangential slip function in (36) becomes

$$\frac{\mathrm{d}}{\mathrm{d}\tau}g_t = v\mathbf{e}_t^T\left(\hat{\mathbf{V}} + \hat{\dot{\mathbf{z}}}\right) + \frac{g_n\|\mathbf{t}^0\|}{c}\mathbf{e}_n^T\left(\mathbf{V}_{c,\xi} + \dot{\mathbf{z}}_{c,\xi}\right) +$$

$$\frac{\beta^0 g_t - \|\mathbf{t}^0\|^2}{c^0}\mathbf{e}_t^{0^T}\left(\hat{\mathbf{V}} + \hat{\dot{\mathbf{z}}}^0\right) +$$

$$\frac{g_n^0\left[\beta^0\left(\xi_c - \xi_c^0\right) - \|\mathbf{t}^0\|\right]}{c^0}\mathbf{e}_n^{0^T}\left(\mathbf{V}_{c,\xi} + \dot{\mathbf{z}}_{c,\xi}^0\right) +$$

$$(\xi_c - \xi_c^0)\mathbf{e}_t^{0^T}\left(\mathbf{V}_{c,\xi} + \dot{\mathbf{z}}_{c,\xi}^0\right)\,. \tag{66}$$

Thus, the material derivative of the tangential slip function at time $t_n$ depends on quantities at configuration at time $t_{n-1}$ which makes the problem path dependent.

Using (66), the material derivative of the tangential stick variational form in (44) at the perturbed configuration becomes

$$\frac{\mathrm{d}}{\mathrm{d}\tau}b_T(\mathbf{r},\overline{\mathbf{r}}) = b_T^*(\mathbf{r};\dot{\mathbf{r}},\overline{\mathbf{r}}) + b_T'(\mathbf{r},\overline{\mathbf{r}})\,, \tag{67}$$

where $b_T^*(\mathbf{r};\dot{\mathbf{r}},\overline{\mathbf{r}})$ is same as the tangential stick bilinear form in (51) by replacing $\Delta\mathbf{r}$ with $\dot{\mathbf{r}}$ and $b_T'(\mathbf{r},\overline{\mathbf{r}})$ is the tangential stick fictitious load form defined as

$$b_T'(\mathbf{r},\overline{\mathbf{r}}) = b_T^*(\mathbf{r};\mathbf{V},\overline{\mathbf{r}}) +$$

$$\omega_t\int_{\Gamma_c}\frac{2g_t\|\mathbf{t}\|}{c}\hat{\overline{\mathbf{z}}}^T\mathbf{e}_t\mathbf{e}_t^{0^T}\left(\mathbf{V}_{c,\xi} + \dot{\mathbf{z}}_{c,\xi}^0\right)\,\mathrm{d}\Gamma +$$

$$\omega_t\int_{\Gamma_c}v\left(2\beta^0 g_t - \|\mathbf{t}^0\|^2\right)\hat{\overline{\mathbf{z}}}^T\mathbf{e}_t\mathbf{e}_t^{0^T}\left(\hat{\mathbf{V}} + \hat{\dot{\mathbf{z}}}^0\right)\,\mathrm{d}\Gamma +$$

$$\omega_t\int_{\Gamma_c}\frac{\beta^0 g_n g_t\left(\|\mathbf{t}^0\| + \|\mathbf{t}\|\right)}{cc^0}\hat{\overline{\mathbf{z}}}^T\mathbf{e}_t\mathbf{e}_n^{0^T}\left(\mathbf{V}_{c,\xi} + \dot{\mathbf{z}}_{c,\xi}^0\right)\,\mathrm{d}\Gamma -$$

$$\omega_t\int_{\Gamma_c}\frac{g_n\|\mathbf{t}\|\|\mathbf{t}^0\|^2}{cc^0}\hat{\overline{\mathbf{z}}}^T\mathbf{e}_t\mathbf{e}_n^{0^T}\left(\mathbf{V}_{c,\xi} + \dot{\mathbf{z}}_{c,\xi}^0\right)\,\mathrm{d}\Gamma +$$

$$\omega_t\int_{\Gamma_c}\frac{g_n\|\mathbf{t}^0\|\left(2\beta^0 g_t - \|\mathbf{t}^0\|^2\right)}{cc^0}\overline{\mathbf{z}}_{c,\xi}^T\mathbf{e}_n\mathbf{e}_t^{0^T}\left(\hat{\mathbf{V}} + \hat{\dot{\mathbf{z}}}^0\right)\,\mathrm{d}\Gamma +$$

$$\omega_t\int_{\Gamma_c}\frac{g_n g_n^0\left(2\beta^0 g_t - \|\mathbf{t}^0\|^2\right)}{cc^0}\overline{\mathbf{z}}_{c,\xi}^T\mathbf{e}_n\mathbf{e}_n^{0^T}\left(\mathbf{V}_{c,\xi} + \dot{\mathbf{z}}_{c,\xi}^0\right)\,\mathrm{d}\Gamma +$$

$$\omega_t\int_{\Gamma_c}\kappa\left(vg_t\hat{\overline{\mathbf{z}}}^T\mathbf{e}_t + \frac{g_n g_t\|\mathbf{t}^0\|}{c}\hat{\overline{\mathbf{z}}}^T\mathbf{e}_t\right)(\mathbf{V}^T\mathbf{n})\,\mathrm{d}\Gamma\,. \tag{68}$$

### 3.2.2
### DSA formulation for slip condition

The material derivative of (46) can be taken using the similar procedure as in the stick condition, except the normal gap function, to obtain (67) where $b_T^*(\mathbf{r};\dot{\mathbf{r}},\overline{\mathbf{r}})$ is obtained from the tangential slip bilinear form in (53) by replacing $\Delta\mathbf{r}$ with $\dot{\mathbf{r}}$ and $b_T'(\mathbf{r},\overline{\mathbf{r}})$ is the tangential slip fictitious load form defined as

$$b_T'(\mathbf{r},\overline{\mathbf{r}}) = b_T^*(\mathbf{r};\mathbf{V},\overline{\mathbf{r}}) +$$

$$\omega_t \int_{\Gamma_c} \frac{g_n\|\mathbf{t}\|}{c}\hat{\overline{\mathbf{z}}}^T\mathbf{e}_t\mathbf{e}_t^{0^T}\left(\mathbf{V}_{c,\xi}+\dot{\mathbf{z}}_{c,\xi}^0\right)\mathrm{d}\Gamma +$$

$$\omega_t \int_{\Gamma_c} \frac{v\beta^0 g_n}{c^0}\hat{\overline{\mathbf{z}}}^T\mathbf{e}_t\mathbf{e}_t^{0^T}\left(\hat{\mathbf{V}}+\hat{\dot{\mathbf{z}}}^0\right)\mathrm{d}\Gamma +$$

$$\omega_t \int_{\Gamma_c} \frac{\beta^0 g_n g_n^0\|\mathbf{t}^0\|}{cc^0}\hat{\overline{\mathbf{z}}}^T\mathbf{e}_t\mathbf{e}_n^{0^T}\left(\mathbf{V}_{c,\xi}+\dot{\mathbf{z}}_{c,\xi}^0\right)\mathrm{d}\Gamma +$$

$$\omega_t \int_{\Gamma_c} \frac{g_n^2}{c}\overline{\mathbf{z}}_{c,\xi}^T\mathbf{e}_n\mathbf{e}_t^{0^T}\left(\mathbf{V}_{c,\xi}+\dot{\mathbf{z}}_{c,\xi}^0\right)\mathrm{d}\Gamma +$$

$$\omega_t \int_{\Gamma_c} \frac{\beta^0\|\mathbf{t}^0\|g_n^2}{cc^0}\overline{\mathbf{z}}_{c,\xi}^T\mathbf{e}_n\mathbf{e}_t^{0^T}\left(\hat{\mathbf{V}}+\hat{\dot{\mathbf{z}}}^0\right)\mathrm{d}\Gamma +$$

$$\omega_t \int_{\Gamma_c} \frac{\beta^0 g_n^2 g_n^0}{cc^0}\overline{\mathbf{z}}_{c,\xi}^T\mathbf{e}_n\mathbf{e}_n^{0^T}\left(\mathbf{V}_{c,\xi}+\dot{\mathbf{z}}_{c,\xi}^0\right)\mathrm{d}\Gamma +$$

$$\omega_t \int_{\Gamma_c} \kappa\left(vg_n\hat{\overline{\mathbf{z}}}^T\mathbf{e}_t + \frac{g_n^2\|\mathbf{t}^0\|}{c}\overline{\mathbf{z}}_{c,\xi}^T\mathbf{e}_n\right)(\mathbf{V}^T\mathbf{n})\,\mathrm{d}\Gamma\,. \tag{69}$$

Note that the same symbol $b_T'(\mathbf{r},\overline{\mathbf{r}})$ is used for stick and slip conditions. Thus, the material derivative of the contact variational form can be obtained by combining (62), (67), and (68) for the stick condition and (62), (67), and (69) for the slip condition,

$$\frac{\mathrm{d}}{\mathrm{d}\tau}b_{\Gamma_c}(\mathbf{r},\overline{\mathbf{r}}) = b_{\Gamma_c}^*(\mathbf{r};\dot{\mathbf{r}},\overline{\mathbf{r}}) + b_V'(\mathbf{r},\overline{\mathbf{r}})\,, \tag{70}$$

where

$$b_{\Gamma_c}^*(\mathbf{r};\dot{\mathbf{r}},\overline{\mathbf{r}}) = b_N^*(\mathbf{r};\dot{\mathbf{r}},\overline{\mathbf{r}}) + b_T^*(\mathbf{r};\dot{\mathbf{r}},\overline{\mathbf{r}})\,, \tag{71}$$

$$b_V'(\mathbf{r},\overline{\mathbf{r}}) = b_N'(\mathbf{r},\overline{\mathbf{r}}) + b_T'(\mathbf{r},\overline{\mathbf{r}})\,. \tag{72}$$

Thus, if all the terms regarding the material derivative of variational (57) is collected, then the following linear system of equations can be obtained

$$a_\Omega^*({}^n\mathbf{r};{}^n\dot{\mathbf{r}},\overline{\mathbf{r}}) + b_{\Gamma_c}^*({}^n\mathbf{r};{}^n\dot{\mathbf{r}},\overline{\mathbf{r}}) =$$

$$\ell_V'(\overline{\mathbf{r}}) - a_V'({}^n\mathbf{r},\overline{\mathbf{r}}) - b_V'({}^n\mathbf{r},\overline{\mathbf{r}})\,, \quad \forall\overline{\mathbf{r}}\in Z\,. \tag{73}$$

The left side of (73) is the same form as in (55). Thus, the same decomposed stiffness matrix can be used for computation of the material derivative of the displacement with the fictitious load. Since the tangent stiffness operator in (55) is not symmetric, the direct differentiation method is more suitable. Since the tangential slip fictitious load depends on the material derivative of the previous converged configuration, the linear system (73) is solved at each load step. Sensitivity computation does not require convergence iterations; only the stiffness matrix at the converged configuration of each load step is used for linear analysis. Since the contact variational term is independent of structural terms in the sensitivity equation, other types of material model can be treated using (73) if an appropriate derivative form of structure and load are used.

## 4
## Numerical example: Shape DSA and optimization of windshield wiper problem

The continuum-based response analysis (55) and DSA (73) are discretized by reproducing kernel particle method (RKPM) (Chen *et al.* 1998) where the structural domain is represented by finite number of particles. RKPM introduces a modified kernel function that is constructed based on the enforcement of reproducing conditions such that the kernel estimates of displacement variables exactly reproduce polynomials up to certain degree. RKPM is an ideal choice since, unlike the conventional FEA method, the solution is much less sensitive to the mesh distortion which causes many difficulties in large deformation analysis as well as shape optimization.

Figure 4 shows the geometry of the windshield blade and the geometry of the glass with discretized particles of RKPM. Since there is enough difference in stiffnesses between rubber and glass, the glass material is assumed to be rigid compared to the rubber material. For the convenience of analysis, the shape of the rigid wall is approximated as a straight line, and a vertical geometry of the rigid wall is added for smooth deformation of the contact region. The upper part of the blade is supported by a steel slab. The material constants and contact parameters are shown in Table 1.

**Table 1** Material constants and contact parameters

| | | |
|---|---|---|
| $D_{10} = 80\,\mathrm{kPa}$ | $D_{01} = 20\,\mathrm{kPa}$ | $K = 80\,\mathrm{MPa}$ |
| $\mu = 0.15$ | $\omega_n = 10^7$ | $\omega_t = 10^6$ |

As the rigid body moves to the left, the lead of blade is in contact with the glass, which is modeled as flexible-rigid body contact. The deformation of blade is large

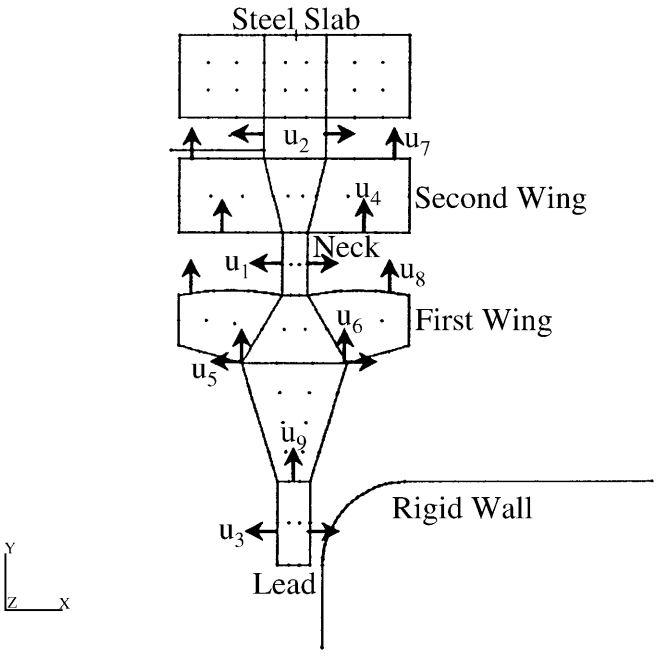


**Fig. 4** Geometry and design parameters of windshield wiper

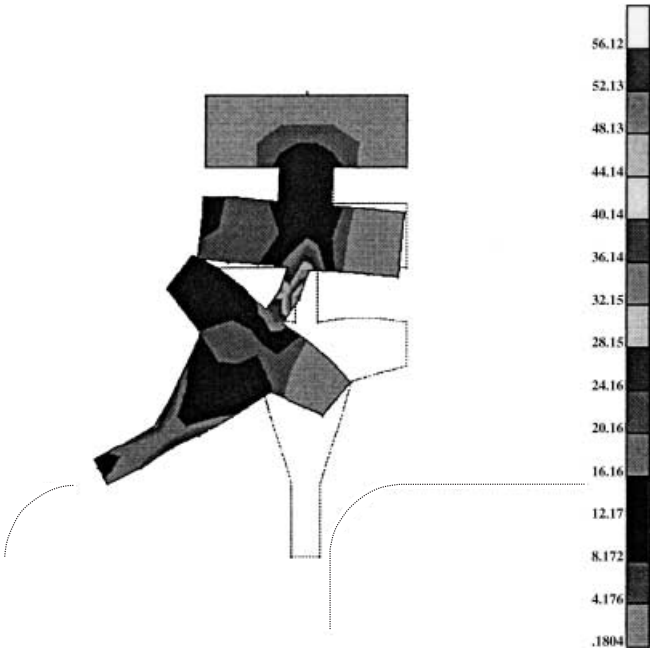


**Fig. 5** Von Mises stress contour plot of windshield wiper

enough that the first wing of the blade is in contact with the second wing of the blade, which is modeled as a flexible-flexible body contact. Also the second wing is in contact with the steel slab, which is modeled as a flexible-rigid body contact. The function of the thin neck is to generate flexibility such that the direction of the blade can be easily turned over when the blade changes its moving direction. The role of wing is to supply enough contact force at the lead point. Figure 5 shows von Mises stress contour plot with the deformed geometry at the final configuration. The stress concentration is found at the neck and the lead because of the bending effect.

The geometry of the structure is parameterized using 9 shape design variables as shown in Fig. 4. The design velocity field at the boundary is obtained first by perturbing the boundary curve corresponding to the design variable, and the domain design velocity field is computed using an isoparametric mapping method (Choi and Chang 1994). Four performance measures are chosen: the total area of structure, two von Mises stresses of the neck region, and the $y$ directional contact force at the lead.

DSA is carried out at each converged load step to compute the material derivative of the displacement. The sensitivities of the performance measures are computed at the final converged load step using the material derivative of the displacement. The cost of sensitivity computation is about 4% of that of response analysis per design parameter, which is quite efficient compared to the finite difference method. The accuracy of the sensitivity is compared with the forward finite difference results for the perturbation size of $\tau = 10^{-6}$. Table 2 shows the accuracy of the sensitivity results. In Table 2, the second column, $\Delta\Psi$ denotes the finite difference results and the third column represents the change of the performance measure from the proposed method. Excellent sensitivity results are obtained.

**Table 2** Sensitivity results and comparison with finite difference method

| Performance | $\Delta\Psi$ | $\Psi'$ | $(\Delta\Psi/\Psi') \times 100$ |
|---|---|---|---|
| $u_1$ | | | |
| Area | .28406E-5 | .28406E-5 | 100.00 |
| $vm_{53}$ | .19984E-3 | .19984E-3 | 100.00 |
| $vm_{54}$ | .28588E-3 | .28588E-3 | 100.00 |
| $F_{cy}$ | .55399E-5 | .55399E-5 | 100.00 |
| $u_3$ | | | |
| Area | .68663E-5 | .68663E-5 | 100.00 |
| $vm_{53}$ | .19410E-3 | .19410E-3 | 100.00 |
| $vm_{54}$ | .68832E-4 | .68832E-4 | 100.00 |
| $F_{cy}$ | .43976E-4 | .43976E-4 | 100.00 |
| $u_5$ | | | |
| Area | .33000E-5 | .33000E-5 | 100.00 |
| $vm_{53}$ | .22762E-4 | .22762E-4 | 100.00 |
| $vm_{54}$ | .77289E-5 | .77286E-5 | 100.00 |
| $F_{cy}$ | .62356E-5 | .62355E-5 | 100.00 |
| $u_6$ | | | |
| Area | −.24000E-5 | −.24000E-5 | 100.00 |
| $vm_{53}$ | −.16452E-4 | −.16452E-4 | 100.00 |
| $vm_{54}$ | .36694E-5 | .36690E-5 | 100.01 |
| $F_{cy}$ | −.26072E-5 | −.26072E-5 | 100.00 |

The objective of the design problem is to reduce the material of the blade by changing the shape of the blade. The stress concentration is to be reduced and the contact

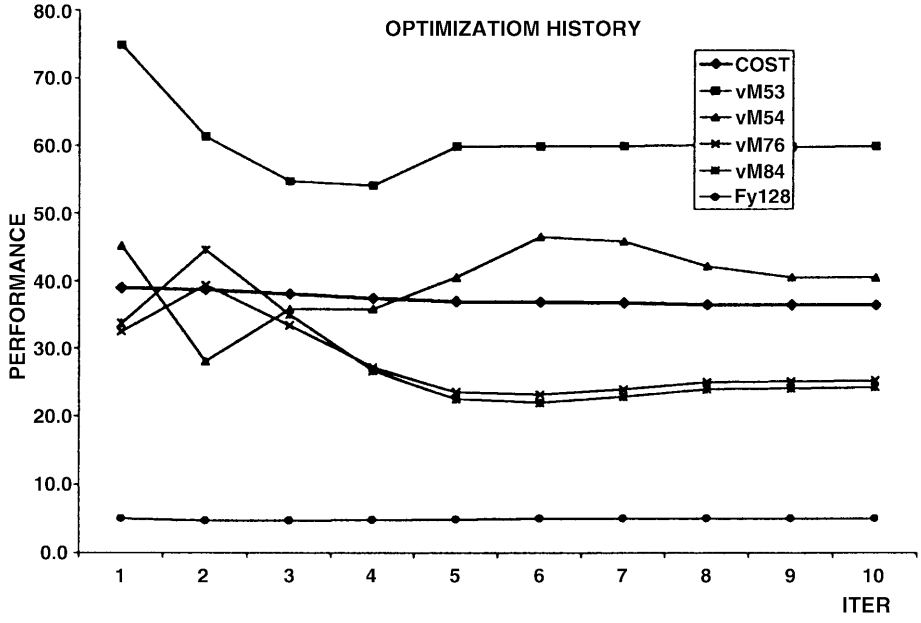


**Fig. 6** Optimization history of windshield wiper contact problem

force at the lead is to be increased at the same time. The design optimization problem is

$$\min \text{ Area}(39)\,,$$

$$\text{s.t. } \sigma_{53}(75), \sigma_{54}(45), \sigma_{76}(32), \sigma_{84}(34) \leq 55\,,$$

$$F_{y128}(5) \geq 5.5\,,$$

$$-0.2 \leq u_i \leq 0.2\,, \quad i = 1, 3, 7, 8\,,$$

$$-0.3 \leq u_i \leq 0.3\,, \quad i = 2, 4\,,$$

$$-0.6 \leq u_i \leq 0.6\,, \quad i = 5, 6\,,$$

$$-0.1 \leq u_i \leq 0.1\,, \quad i = 9\,, \tag{74}$$

where the values within the parenthesis are the original response values. Design optimization is carried out using the sequential quadratic programming method. The performance values are supplied to the optimizer by solving nonlinear analysis (RKPM) and the sensitivity coefficients are provided by the proposed method. Optimization is converged after 10 iterations and Fig. 6 shows the history of the cost and constraint functions. The cost function, which is the total area, is reduced by 3.5%. Figure 7 shows the optimized geometry and the analysis result. As shown in the figure, the thickness of the lead is increased to increase the contact force, whereas the thickness of the neck is reduced to decrease the bending stress at that region. The thickness of the first wing is reduced to the lower bound since the level of the stress is relatively low.

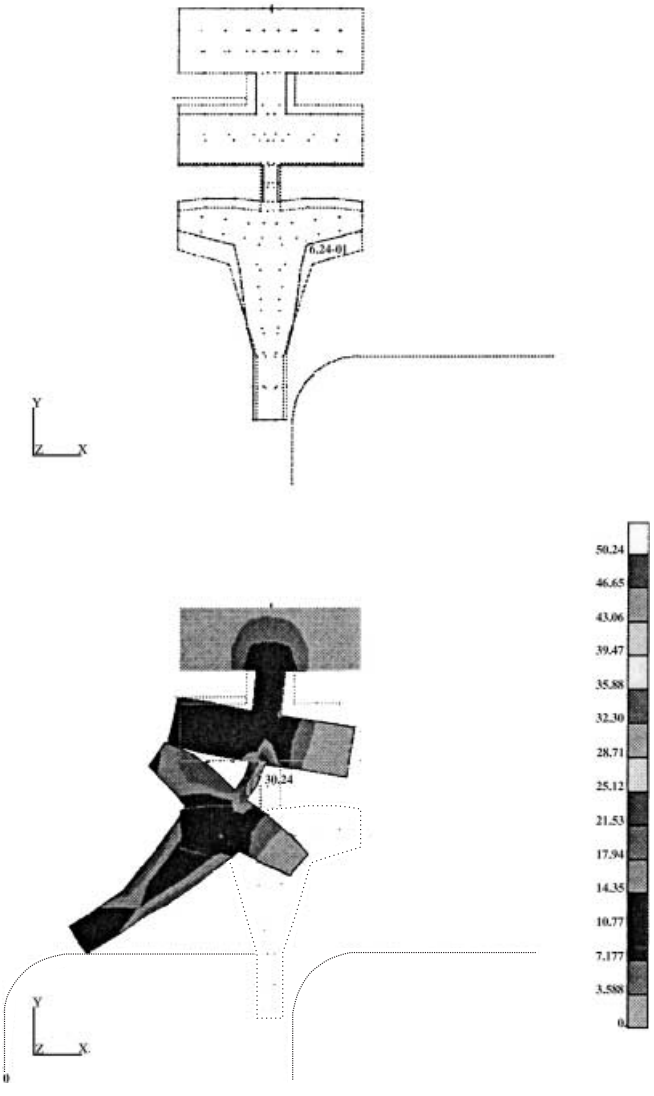


**Fig. 7** Optimized shape design and analysis result

## 5 Conclusions

A continuum-based shape design sensitivity formulation of the multibody frictional contact problem for hyper-elastic material is developed. DSA uses the same tangent stiffness matrix as analysis at the converged configuration. No convergence iterations are required for sensitivity computation, and thus sensitivity analysis takes much less effort than nonlinear response analysis. It is also demonstrated that shape optimization of the multibody frictional contact problem can be performed efficiently due to accuracy of the design sensitivity of the continuum-based DSA method.

*Acknowledgements* This research was partially supported by the NSF/DARPA OPAAL (DMS 98-74015) and Ford University Research Program (URP 97-723R). These supports are gratefully acknowledged.

## References

Antunez, H.J.; Kleiber, M. 1996: Sensitivity analysis of metal forming process involving frictional contact in steady state. *Materials Proc. Tech.* **60**, 485–491

Chen, J.S.; Pan, C.; Wu, C.T. 1998: Application of reproducing kernel particle method to large deformation contact analysis of elastomers. *Rubber Chem. Tech.* **71**, 191–213

Chen, J.S.; Wu, C.T.; Pan, C. 1996: A pressure projection method for nearly incompressible rubber hyper-elasticity. Part I: Theory. Part II: Application. *ASME J. Appl. Mech.* **63**, 862–876

Choi, K.K.; Chang, K.H. 1994: A study on the velocity computation for shape design optimization. *J. Finite Elements Anal. Des.* **15**, 317–347

Choi, K.K.; Kim, N.H.; Park, Y.H. 1998: Shape design sensitivity analysis for contact problem with friction. *Proc. 7-th AIAA/USAF/NASA/ISSMO Symp. on Multidisciplinary Analysis and Optimization* (held in St. Louis, MO), pp. 1071–1081

Grindeanu, I.; Chang, K.H.; Choi, K.K.; Chen, J.S. 1998: Design sensitivity analysis of hyper-elastic structures using a meshless method. *AIAA J.* **36**, 618–627

Haraux, A. 1977: How to differentiate the projection on a convex set in Hilbert space. Some applications to variational inequalities. *J. Math. Soc. Japan* **29**, 615–631

Haug, E.J.; Choi, K.K.; Komkov, V. 1986: *Design sensitivity analysis of structural systems*. New York: Academic Press

Hughes, T.J.R. 1987: *The finite element method*. Englewood Cliffs: Prentice-Hall

Malkas, D.S.; Hughes, T.J.R. 1978: Mixed finite element methods-reduced and selective integration techniques: A unification of concept. *Comp. Meth. Appl. Mech. Engrg.* **15**, 63–81

Mignot, F. 1976: Controle dans les inequations variationelles elliptiques. *J. Func. Anal.* **22**, 130–185

Oden, J.T.; Kikuchi, N. 1982: Finite element methods for constrained problems in elasticity. *Int. J. Numer. Meth. Engrg.* **18**, 701–725

Pollock, G.D.; Noor, A.K. 1996: Sensitivity analysis of the contact/impact response of composite structures. *Comp. Struct.* **61**, 251–269

Santos, J.L.T.; Choi, K.K. 1992: Shape design sensitivity analysis of nonlinear structural systems. *Struct. Optim.* **4**, 23–35

Sokolowski, J.; Zolesio, J.P. 1991: *Introduction to shape optimization*. Berlin, Heidelberg, New York: Springer

Spivey, C.O.; Tortorelli, D.A. 1994: Tangent operators, sensitivity expressions, and optimal design of non-linear elastica in contact with applications to beams. *Int. J. Numer. Meth. Engrg.* **37**, 49–73

Sussman, T.; Bathe, K. J. 1987: A finite element formulation for nonlinear incompressible elastic and inelastic analysis. *Comp. Struct.* **26**, 357–409

Wriggers, P.; Van, T.V.; Stein, E. 1990: Finite element formulation of large deformation impact-contact problems with friction. *Comp. Struct.* **37**, 319–331